The Joint Effect of Mid-latitude Winds and the Westerly Quasi-Biennial Oscillation Phase on the Antarctic Stratospheric Polar Vortex and Ozone

Zhe Wang[1], Jiankai Zhang[1*], Siyi Zhao[1], Douwang Li[1]

[1]Key Laboratory for Semi-Arid Climate Change of the Ministry of Education, School of Atmospheric Sciences, Lanzhou University, Lanzhou, 730000, China.

Correspondence to: Jiankai Zhang (jkzhang@lzu.edu.cn)

Abstract. The quasi-biennial oscillation (QBO) dynamically interacts with the extratropical atmosphere. However, the relationship between the QBO in austral winter and the Antarctic stratospheric polar vortex in spring remains unclear. Here, we proposed a joint predictor involving the QBO for the Antarctic polar vortex and ozone in austral spring. During the westerly QBO phase (WQBO), positive anomalies in the zonal-mean zonal wind at 20°S−40°S in the upper stratosphere in July, named as the positive extratropical mode, can lead to a stronger Antarctic stratospheric polar vortex and lower ozone concentration in November, with correlations reaching 0.75 and 0.60, respectively. The mechanism is summarized as follows: the positive extratropical mode triggers a secondary circulation, which further alters the environmental condition for wave propagation in the stratosphere, pushing the positive zonal-mean zonal wind anomalies towards the pole. While during the easterly QBO phase (EQBO), the correlation of the extratropical mode and the strength of polar vortex is only 0.1. Due to stronger upward motions in the tropics, which opposes the secondary circulation caused by the extratropical mode, the EQBO cannot sustain the positive anomalous zonal-mean zonal wind until November. Our results highlight that the extratropical mode during WQBO could serve as a reliable predictor of the Antarctic stratospheric polar vortex and Antarctic ozone hole with a five-month time lag.

1 Introduction

The quasi-biennial oscillation (QBO) is a dominant mode of interannual variability in the tropical stratosphere (Lindzen and Holton 1968; Andrews and McIntyre 1976; Baldwin et al. 2001; Anstey and Shepherd, 2014; Yamashita et al., 2018; Rao et al., 2019; 2020a; 2023a). It is a quasi-periodic oscillation of the equatorial zonal wind, alternating between easterlies and westerlies in the tropical stratosphere, with a mean period of approximately 28 months. (Lindzen and Holton, 1968; Andrews and McIntyre, 1976; Baldwin et al., 2001). The QBO plays a crucial role in influencing atmospheric circulation and chemical species outside the tropical stratosphere (Holton and Tan, 1980; Ruti et al., 2006; Garfinkel and Hartmann, 2011; Yamashita et al., 2015; Gray et al., 2018; Rao et al., 2019; 2020a, b, c; Zhang et al., 2021). Holton and Tan (1980) proposed that QBO can modify upward-propagating planetary waves by altering the zero-wind line in the stratosphere, which further affects the extratropical waveguide (Baldwin et al., 2001; Anstey et al., 2014; Zhang et al., 2019). During the westerly QBO phase (WQBO), the zero-wind line of the zonal-mean zonal wind shifts equatorward. This causes planetary wave to be reflected

away from high latitudes, leading to a strengthened polar vortex by reducing wave-driven disturbances in the polar region. Consequently, the Arctic stratospheric polar vortex tends to be stronger on average during the WQBO compared to the easterly QBO phase (EQBO). Additionally, Garfinkel et al. (2012) proposed that the secondary meridional circulation induced by the EQBO also plays a crucial role in the Arctic stratosphere. This secondary circulation restricts the propagation of subpolar Rossby waves into the subtropics, resulting in more wave breaking closer to the pole. This QBO-induced changes in the Arctic stratospheric polar vortex can further influence the distribution of Arctic ozone and water vapor (Wang et al., 2022; Lu et al., 2023). Zhang et al. (2021) revealed that dynamical processes play a more important role in the Arctic ozone-QBO connection than chemical processes, although the impact of chemical processes on the Arctic ozone-QBO signal is not negligible. Furthermore, observational and modeling evidences both show that the QBO's influence on the Arctic stratospheric polar vertex and ozone occurs within the extended winter (November–March; Rao et al., 2019; 2020b; Zhang et al., 2021).

In the Southern Hemisphere (SH), upward-propagating planetary waves are weak due to the less topography and the weaker thermal contrast between land and sea. Consequently, the QBO-vortex coupling, which is closely related to planetary waves, has received less attention than those in the Northern Hemisphere (NH, Garcia and Solomon, 1987; Lait et al., 1989; Baldwin and Dunkerton, 1998; Naito, 2002; Hitchman and Huesmann, 2009; Yamashita et al. 2018; Rao et al., 2023a and b). Naito et al. (2002) examined the QBO signal in the SH and found that from September to October, the zonal-mean zonal wind in the lower stratosphere decelerates more rapidly during the EQBO than WQBO. This deceleration is attributed to the stronger upward wave propagation from the troposphere and larger wave convergence during the EQBO in these two months. However, Anstey et al. (2014) demonstrated that the extratropical response to the QBO occurs in November, interpreted as the modulation of the Antarctic polar vortex's final warming. Thus, it remains unclear when the response of Antarctic stratospheric polar vortex to the QBO reaches its peak. Yamashita et al. (2018) examined the influence of the QBO on SH extratropical circulation from austral winter to early summer using a multiple linear regression approach. Their findings suggest that the QBO-SH polar vortex connection operates through two distinct pathways: the mid-stratospheric pathway, which tends to suppress the propagation of planetary waves into the stratosphere during WQBO, and the low-stratospheric pathway, which tends to enhance upward planetary waves in EQBO. The QBO-SH polar vortex connections established by Yamashita et al. (2018) are statistically significant. However, in QBO-resolving models from phases 5/6 of the Coupled Model Intercomparison Project (CMIP5/6), fewer than half of the General Circulation Models (GCM) successfully reproduce a weakened SH polar vortex during EQBO (Rao et al., 2023b). Furthermore, they also suggest that even the high-skill models capture only about 30% of the observed deceleration in westerlies during the EQBO. Although previous studies have revealed the potential relationship and mechanisms linking the QBO with the Antarctic stratospheric polar vortex, the weak statistical correlation between them and the limited performance of GCMs indicate that the QBO-vortex coupling in the SH is not yet fully understood. In addition to the Antarctic stratospheric polar vortex, previous studies have also investigated the QBO signals in stratospheric ozone. Garcia and Solomon (1897) demonstrated that the year-to-year fluctuations in Antarctic ozone may be linked to the tropical QBO. In contrast, Wang et al. (2022) suggested that the Antarctic total column ozone (TCO) shows no significant response to

65   the QBO signal (Figure 2 in Wang et al., 2022). So far, the impacts of the QBO on the Antarctic stratospheric polar vortex and ozone have not been well documented.

The QBO period varies irregularly in the range from 17 to 38 months, which is considered as a reliable predictor of the stratospheric polar vortex, and further the near-surface weather and climate in the NH (Baldwin and Dunkerton, 2001; Zhang et al., 2020; Tian et al., 2023). In the SH, if the QBO-vortex coupling does exist, it could also serve as a predictor for the

70   Antarctic stratospheric polar vortex and ozone. In this study, we aim to explore when and how the QBO influences the SH stratospheric polar vortex. Understanding this connection between the QBO and high-latitude circulation may help improve the forecasting accuracy of the SH stratospheric polar vortex, and, by extension, the Antarctic ozone hole. Section 2 presents the data and methods used in this research. In Section 3, we propose an improved predictor for the Antarctic stratospheric polar vortex and ozone based on the QBO. We also discuss the underlying mechanisms. The conclusions are provided in section 4.

75   **2 Data and methods**

2.1 Data

Monthly and daily meteorological data and ozone volume mixing ratio are derived from Modern-Era Retrospective analysis for Research and Applications, Version 2 (MERRA-2; GMAO, 2015) reanalysis for the period from 1980 to 2022. The reanalysis data has a resolution of 1.25°×1.25° and 42 pressure levels extending from 1000 to 0.1 hPa. The Polar Stratospheric

80   Cloud (PSC) area is obtained from the NASA ozone watch website.

Previous studies have employed different methods to define the QBO index. Some are based on the tropical zonal-mean zonal wind at a single pressure level (Holton and Tan, 1980; Gray et al., 1992; Baldwin et al., 2001; Garfinkel and Hartmann, 2007), while others use two QBO indices on different pressure levels (Andrews et al., 2019) or use empirical orthogonal function (EOF) analysis applied on the tropical zonal-mean zonal wind (Randel et al., 1999; Anstey et al., 2010; Rao and Ren,

85   2018), which can better capture QBO's vertical structure. The QBO phase defined by the EOF method is similar to that defined by the single pressure level QBO index (Baldwin et al., 2001; Rao et al., 2020b). Typically, when tropical stratosphere winds near 50 hPa are used to define the QBO phase, the NH stratospheric polar vortex during winter tends to strengthen during the WQBO and weaken during the EQBO (Baldwin et al. 2001; Anstey and Shepherd, 2014; Anstey et al., 2022). In the SH, the Antarctic stratospheric polar vortex shows responses to the tropical winds around 20 hPa (Baldwin and Dunkerton 1998;

90   Baldwin et al., 2001; Baldwin and Dunkerton 1998; Anstey et al., 2022; Rao et al., 2023b). Therefore, this study uses the standardized zonal-mean zonal wind averaged over 10°S−10°N at 20 hPa to define the QBO phase. The EQBO phase is defined as years when the tropical standardized zonal-mean zonal wind is less than −1, while the WQBO corresponds to years when the tropical standardized zonal-mean zonal wind is greater than 1. The El Nino-Southern Oscillation (ENSO) index is defined as the sea surface temperature (SST) anomalies averaged over the Niño 3.4 region (5°N−5°S; 170°−120°W). SST is derived

95   from the monthly NOAA Extended Reconstruction SSTs Version 5 (ERSSTv5).

2.2 Method

2.2.1 Singular value decomposition (SVD)

The SVD analysis is performed between the zonal-mean zonal wind at latitudes ranging from 0° to 40°S and 1−70 hPa in July (extratropical mode) and the zonal-mean zonal wind at latitudes ranging from 50°S to 70°S and 1−70 hPa in November (polar mode). To validate the robustness of the findings, we conduct a Monte Carlo test (Iwasaka and Wallace, 1995) by creating 1000 ensembles of the SVD analysis. In this test, the tropical wind field is kept fixed, while the polar wind is randomly disordered in both time and space. The total variance of the 1000 paired ensembles is calculated and sorted. If the observed SVD total variance exceeds the 95th percentile of the ensemble distribution, the SVD mode is considered significant at the 95% confidence level.

2.2.2 Eliassen-Palm (E-P) flux and stream function

The E-P flux (Andrews et al., 1987) is used to diagnose the propagation of waves, which is calculated as follows:

$$F_\varphi \equiv \rho_0 a cos\varphi \left(\frac{\overline{u_z} \overline{v'\theta'}}{\overline{\theta}_z} - \overline{u'v'} \right) \tag{1}$$

$$F_z \equiv \rho_0 a cos\varphi \left\{ \left[f - \left(a cos\varphi \right)^{-1} \left(\overline{u} cos\varphi \right)_\varphi \right] \frac{\overline{v'\theta'}}{\overline{\theta}_z} - \overline{w'u'} \right\} \tag{2}$$

$$\nabla \cdot F \equiv \left(a cos\varphi \right)^{-1} \frac{\partial}{\partial \varphi} \left(F_\varphi cos\varphi \right) + \frac{\partial F_z}{\partial z} \tag{3}$$

Where ρ_0 is the density; z is the altitude; a is the radius of the Earth; φ is the latitude; f is the Coriolis parameter; θ is the potential temperature; u and v are the zonal and meridional winds, respectively; w is the vertical velocity. The overbars represent the zonal average, and primes represent deviation from the zonal average.

Mass stream function $\overline{\chi}*$ associated with the residual circulation is defined as:

$$\frac{\partial \overline{\chi}*}{\partial \varphi} = \rho_0 a \cos\varphi \overline{w}* \tag{4}$$

Where $\overline{w}*$ is represented as:

$$\overline{w}* = \overline{w} + (a\cos\varphi)^{-1} (\frac{\cos\varphi \overline{v'\theta'}}{\overline{\theta}_z})_\varphi \tag{5}$$

In the SH, the climatological mean mass stream function is negative.

2.2.3 The refraction index

We use the method developed by Harnik and Lindzen (2001) to divided the traditional refraction index (n_{ref}^2) into vertical (m^2)

and meridional components (l^2) by solving the quasi-geostrophic equations in the spherical coordinates:

$$\frac{\partial^2 \psi}{\partial z^2} + \frac{N^2}{f^2}\frac{\partial^2 \psi}{\partial y^2} + n_{ref}^2 \psi = 0 \tag{6}$$

Where ψ is the weighted wave geopotential height, and N^2 is the Brunt-Väisälä frequency. By solving Eq. (6), the vertical

and meridional components of the refraction index can be expressed as:

$$\mathrm{Re}(\frac{\psi_{zz}}{\psi}) = -m^2 \ \text{ and } \ \mathrm{Re}(\frac{\psi_{yy}}{\psi}) = -l^2 \tag{7}$$

And regions with a large refraction index facilitate wave-propagation.

2.2.4 The Lorenz energy cycle

The Lorenz energy cycle is used here to measure the atmospheric circulation changes. As described by Lorenz (1967) and

Holton (1968), the diabatic heating generates mean available potential energy (PM), which is described as (Hu et al., 2004):

$$PM = \frac{c_p}{2}\int \gamma [<T>]''^2 \, dm \tag{8}$$

$$\gamma = -\{\frac{\theta}{T}[(\frac{R}{c_p})p]\} \tag{9}$$

And then the baroclinic eddies transport warm air poleward, cold air equatorward, and transform the PM to eddy available

potential energy (PE). At the same time, the PE is transformed into eddy kinetic energy (KE) by the vertical motions of the

eddies, and the KE can be described as:

$$KE = \frac{1}{2}\int [<u^2> + <v^2>]dm + \frac{1}{2}\int [<u>^{*2} + <v>^{*2}]dm \tag{10}$$

The mean kinetic energy (KM), defined as the integration of $\overline{u}^2$, can be maintained primarily by the conversions from

KE due to the correlation $\overline{u'v'}$ (Eq. 11). Additionally, it can also be converted into the PM (Eq. 12).

$$C(KE,\ KM) = \int [<u^{'}v^{'}> + <u>^{*}<v>^{*}]\cos\varphi\{\frac{\partial([<u>]/\cos\varphi)}{a\partial\varphi}\}dm$$

$$+ \int [<v^{'2}> + <v>^{*2}]\frac{\partial[<v>]}{a\partial\varphi}dm$$

$$+ \int [<u^{'}w^{'}> + <u>^{*}<w>^{*}]\frac{\partial[<u>]}{\partial p}dm \qquad (11)$$

$$+ \int [<v^{'}w^{'}> + <v>^{*}<w>^{*}]\frac{\partial[<v>]}{\partial p}dm$$

$$- \int [<v>][<u^{'2}> + <u>^{*2}]\frac{[tan\varphi]}{a}dm$$

$$C(KM,\ PM) = \int [<v>]g\frac{\partial[<z>]}{a\partial\varphi}dm \qquad (12)$$

Where T is the temperature, c_p is the specific heat of air at constant pressure, p is pressure, R is the gas constant for dry air, and g is the gravitational acceleration. The $<>$ and $[\ ]$ are represent the time and zonal average. The $*$ and $'$ denote the departure from zonal mean and time average. The $"$ represents departure from meridional average. $C(A,\ B)$ represents the conversion from A to B. The $\int[s]dm$ is defined as $\int_{z}\int_{y}\int_{x}s\rho_0\ dx\ dy\ dz$.

2.3 Model simulation

In this study, we use the Whole Atmosphere Community Climate Model (WACCM) in the Community Earth System Model version 2 (CESM2) to investigate the connection between the QBO signal and the Antarctic polar vortex state. The model has a horizontal resolution of 1.9° × 2.5° and a hybrid vertical coordinate with 70 levels from the surface to approximately 140 km (Gettelman et al., 2019). To avoid the impact of initial fields and stochastic low-frequency climate fluctuations on the experiment results (Zhang et al., 2024), 20 ensemble experiments were conducted using the same annual cycle of external forcing in 2000 (e.g., sea ice concentration, sea surface temperature, stratospheric ozone and other chemistry species, greenhouse gas, aerosols, and solar radiation) but with different initial fields. The nudging technology uses a dynamical-core-independent scheme (Davis et al., 2022).

$$F = -W\frac{(X - X_{ref})}{\tau} \qquad (13)$$

Where X_{ref} is the meteorology value from reanalysis datasets at the next update step, τ is the relaxation timescale (6 hours), and W is the nudging coefficients from 0 to 1. Stratospheric zonal wind, meridional wind, and temperature from 1.2 to 103.3 hPa are nudged with a nudging coefficient of 1.0. This nudging coefficient decreases linearly to 0 from 103.3 hPa to 143.0 hPa. Tropical stratosphere (22°S to 22°N) is nudged to a coefficient of 1.0, with a transitional latitude of 22°N/S to 35°N/S. The stratospheric conditions mentioned above are nudged to the JRA-55 reanalysis, and each nudging experiment runs from

1980 to 2022. Note that different sets of reanalysis data are used to force the CESM and perform other analysis. The consistency of the results across both datasets indicates the robustness of the findings.

3 Results

3.1 A better predictor for the Antarctic polar vortex and ozone

Here, we use the zonal-mean zonal wind at 60ºS and 70 hPa as an indicator of the strength of the Antarctic stratospheric polar vortex. Figure 1a indicates its time-lag correlation with the QBO index. Anstey and Shepherd (2014) reviewed the impact of QBO on high latitudes, showing stronger westerlies during WQBO, though with weak statistical significance. Lecouffe et al. (2022) suggested that the QBO can modulate the polar vortex strength, characterized by a stronger polar vortex and longer vortex duration during WQBO. Therefore, our analysis focuses on the positive correlations in Fig. 1a, representing a stronger polar vortex during the westerly QBO phase. The QBO-SH polar vortex connection emerges in July and persists until austral late spring, with the effect peaking in November (i.e., the influence of the July QBO on the polar vortex peaks four months later, the influence of the August QBO peaks three months later, and so on). This result is consistent with the previous studies (Baldwin and Dunkerton, 1998; Yamashita et al., 2018). Here, we focus on the earliest QBO signal in the Antarctic stratospheric polar vortex to determine the longest possible prediction lead time. Note that there is a maximum positive correlation between July QBO index and Antarctic polar vortex strength 4 months later, suggesting that the QBO signal in austral winter influences the Antarctic stratospheric polar vortex in austral spring. During austral late spring, the duration of the Antarctic ozone hole is highly correlated with the strength of the polar vortex. Consequently, the QBO in winter potentially serves as a predictor of the Antarctic polar vortex and ozone hole in austral spring. However, this QBO-vortex signal is not statistically significant. We examine the response of the Antarctic stratospheric polar vortex in austral spring to the winter QBO (Fig. 1b). The WQBO in winter (QBO index in July greater than 1) does not consistently lead to a stronger zonal-mean zonal wind in polar regions in spring, and the correction between them is only 0.23. These results suggest that the direct impact of the QBO on the Antarctic polar vortex is weak.

To further explore the robust relationship between the winter QBO and the Antarctic stratospheric polar vortex in spring, we first regressed the zonal-mean zonal wind in winter against the strength of the polar vortex in November during the WQBO. Interestingly, the winter zonal-mean zonal wind around 30ºS in the upper stratosphere highly correlates with the Antarctic polar vortex in November (Figures 2a−c). Additionally, the winter mid-latitude wind also shows a high correlation with the Antarctic ozone in November (Figs. 2d−f). These results suggest that the extratropical zonal-mean zonal wind in the upper stratosphere (hereafter, extratropical mode), along with the WQBO signal in winter, might serve as a joint predictor of the Antarctic polar vortex and ozone in austral spring.

Here, the SVD analysis is further used to depict the relationship between the winter extratropical mode (Fig. 2a) and the Antarctic polar vortex in spring. Figures 3a and b show the first paired mode of zonal mean zonal wind in the extratropic and polar regions, respectively. The extratropical mode is characterized by a positive zonal wind anomaly centered around 30°S,

190 which closely resembles the regression patterns in Fig. 2. In the tropical regions, it displays a weak WQBO signal at 20 hPa (right panel of Fig. 3a). In austral spring polar region (Fig. 3b), it features a positive zonal wind south of 50°S indicating a strong polar vortex. The first paired mode explains 98.2% of the total variance and is significant at the 95% confidence level according to the Monte Carlo test. Since the first paired mode represents the dominant coupled variance, our analysis mainly focuses on the first SVD paired mode. The correlation coefficient between the time series of the two modes is 0.75, which is

195 also significant at the 95% significance level (Fig. 3c). Note that almost all years represented by circles fall into the first and third quadrants in Fig. 3c, suggesting that when the extratropical mode is in its positive (negative) phase, a stronger (weaker) polar vortex will occur four months later. It is worth noting that the blue and yellow circles representing the phase and strength of ENSO show no uniform pattern with the strength of polar vortex in November, suggesting that the strong correlation between the two modes appears to have little connection with ENSO. Moreover, the Antarctic stratospheric ozone in austral

200 spring, which is closely related to the stratospheric polar vortex, also exhibits a high correlation of 0.6 with the extratropical mode in July (Fig. 3c). Thus, we can conclude that the winter extratropical mode, in conjunction with the WQBO, is closely linked to the spring Antarctic polar vortex and ozone.
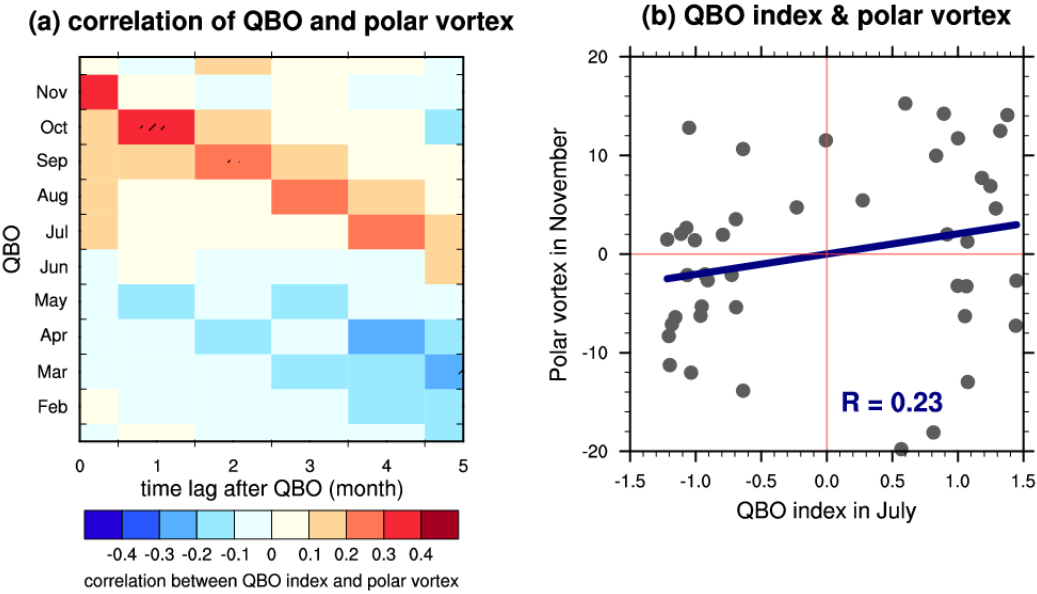
Figure 1: (a) Correlations between the zonal-mean zonal wind at 60°S and 70 hPa and the QBO index at different time lag derived
205 **from the MERRA-2 reanalysis dataset. The Y-axis represents the month of the QBO index used in the correlation analysis. The X-axis indicates the time lags. The shadings indicate that the correlations are statistically significant at 90% confidence level. (b) Monthly mean zonal-mean zonal wind at 60°S and 70 hPa in November (with a 5-month lag after the QBO in July) plotted against the July QBO index according to MERRA-2 reanalysis dataset from 1980 to 2022. The solid blue line represents the linear regression of the QBO index and the strength of Antarctic stratospheric polar vortex, with their correlation coefficient shown in the bottom**
210 **right-hand corner.**
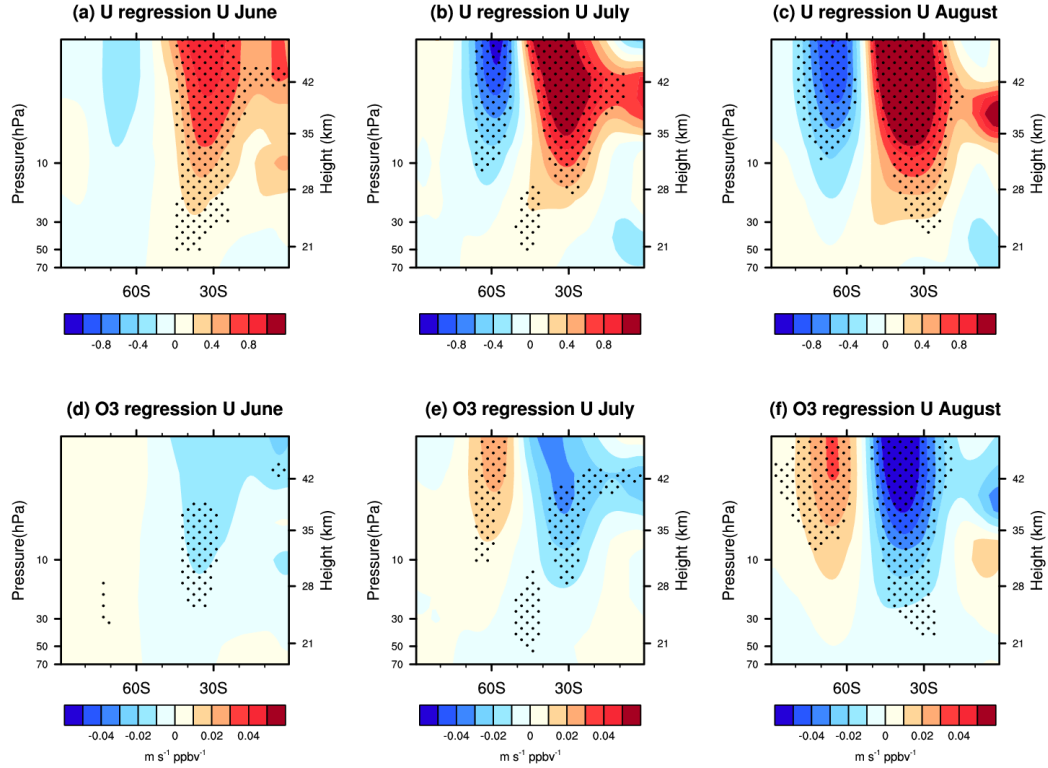
Figure 2: (a)−(c) Regression patterns of the zonal-mean zonal wind in (a) June, (b) July, and (c) August against the zonal-mean zonal wind at 60ºS and 70 hPa in November during WQBO years, derived from the MERRA-2 reanalysis dataset. (d)−(f) Regression patterns of the zonal-mean zonal wind in (d) June, (e) July, and (f) August against the ozone concentration averaged over the south of 60ºS at 70 hPa in November during WQBO years, derived from the MERRA-2 reanalysis dataset. The shadings indicate that the regression coefficients are statistically significant at 95% confidence level.

3.2 The underlying mechanisms responsible for the relationship between the extratropical mode and the Antarctic polar vortex during WQBO

Note that the winter extratropical mode appears early in June and gradually develops (Fig. 2). In July, the extratropical mode is fully formed, and the correlation between the winter extratropical mode and the polar vortex in spring reaches its peak (0.74 in June, 0.75 in July, and 0.73 in August). Therefore, we primarily focus on the relationship between the extratropical mode in July and the Antarctic stratospheric polar vortex in November. As mentioned above, when the extratropical mode in July is in its positive phase (i.e., when the extratropic mode is greater than 0), there is a stronger polar vortex four months later, and vice versa (Fig. 3c). Thus, first we categorize the WQBO into Positive Extratropic mode (Pos-Exmode; 1980, 1990, 2006, 2008, 2015, 2022) and Negative Extratropic mode (Neg-Exmode; 1985, 1997, 2004, 2013, 2016). The Pos-Exmode corresponds to a positive phase of the extratropical mode in July, while Neg-Exmode corresponds to a negative phase (Fig. 3c). A composite analysis is then conducted to compare these two categories.

Figures 4a–e show the difference in composite monthly mean zonal-mean zonal wind between Pos-Exmode and Neg-Exmode from July to November. In the upper stratosphere, a positive center of zonal wind anomalies is located at 20°S–40°S, while a negative center is located at higher latitudes in July. From July to November, the positive zonal-mean zonal wind anomalies exhibit a downward and poleward movement, resulting in a strong polar vortex in austral spring. The negative anomalies also shift towards higher latitudes and gradually weaken, eventually being replaced by positive anomalies in November. The evolution of zonal-mean zonal wind anomalies confirms the connection between the extratropical mode in winter and the polar vortex in November during the WQBO. We further revealed that the positive zonal-mean zonal wind anomalies can be reasonably explained by the E-P flux divergence anomalies and their poleward shift from July to November. The composite differences in E-P flux and its divergence between Pos-Exmode and Neg-Exmode are shown in Figs. 4f–j. In July and August, anomalous E-P flux divergence (Figs. 4f–g) is established between 30°S and 60°S in the upper stratosphere, corresponding to the weaker poleward and upward propagation of planetary waves in this region than normal. These E-P flux divergences lead to the poleward shift of positive zonal-mean zonal wind anomalies from July to August (Figs. 4a–b). Note that the E-P flux divergence anomalies shift to 60°S in the mid and lower stratosphere in September, with these positive anomalies persisting until November.
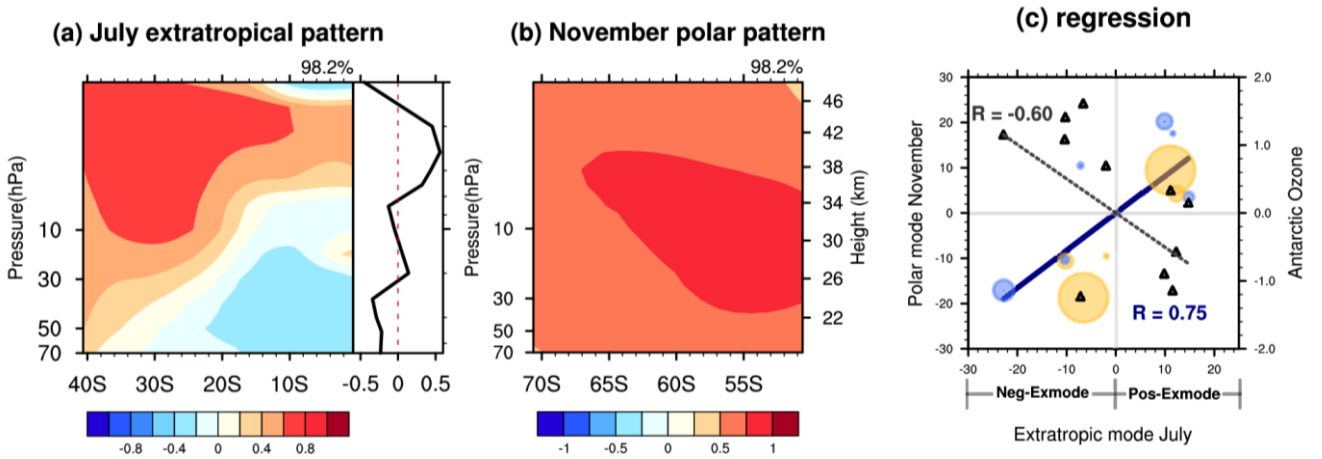
Figure 3: Spatial patterns for the first paired mode of the (a) monthly mean zonal-mean zonal wind over 0−40°S and 1−70 hPa in July, i.e., extratropical mode (b) zonal-mean zonal wind over 50°S−70°S and 1−70 hPa in November by the singular value decomposition (SVD) analysis during WQBO years, based on the MERRA-2 reanalysis dataset from 1980 to 2022. The right panel of (a) is the profile of the extratropical mode averaged over 0−5°S. The variance explained by the first mode is shown in the top right-hand corner. (c) The corresponding time series for the paired mode, with their correlation coefficient shown in the bottom right-hand corner (text in blue). The solid blue line represents the linear regression of the extratropical mode and polar mode. The size and color of the circle markers in panel (c) are proportional to the Niño 3.4 index, with yellow dots indicating a positive Niño 3.4 index and blue dots indicating a negative Niño 3.4 index. The standardized ozone volume mixing ratios, averaged over 60°S−90°S at 70 hPa in November, against the extratropical mode time series are shown in triangular markers (right Y-axis), with their correlation coefficient displayed in the top left-hand corner (text in black). The dashed black line represents the linear regression of the extratropical mode and ozone in November.
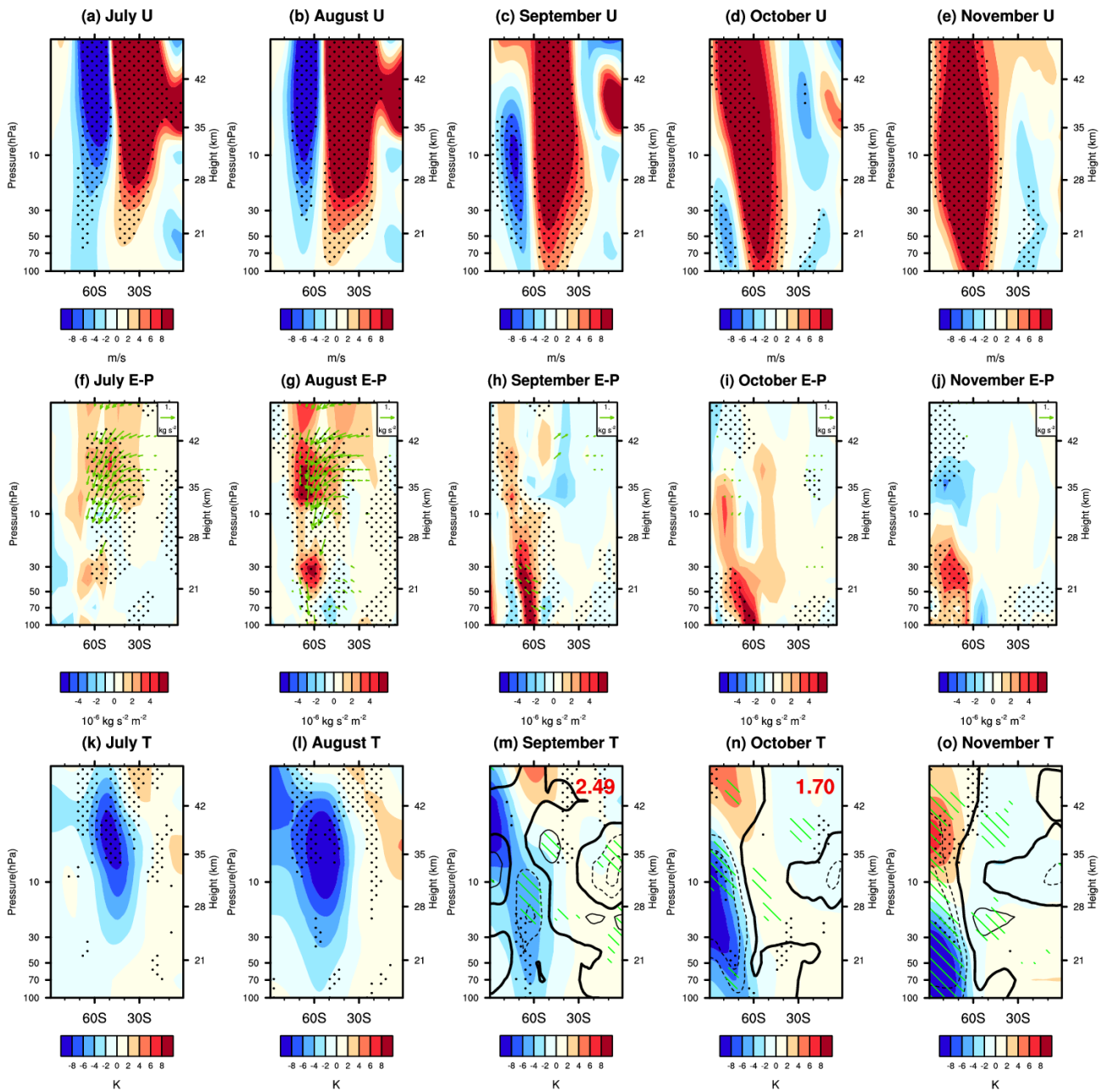
Figure 4: Composite differences in (a)−(e) the zonal-mean zonal wind anomalies, (f)−(j) the scaled E-P flux anomalies (green vectors; horizontal component unit: 10^7 kg s^{-2}; vertical component unit: 10^5 kg s^{-2}) and the E-P flux divergence anomalies (shadings), (k)−(o) the zonal-mean temperature anomalies (shadings) and the zonal-mean ozone volume mixing ratio anomalies (contours; dashed lines are negative, and thick lines are zero contours. The contour intervals are 200 ppbv) from July to November between the Pos-Exmode and Neg-Exmode according to MERRA-2 reanalysis dataset. Composite differences in PSC areas between the Pos-Exmode and Neg-Exmode, based on the NASA ozone watch dataset from September to October, are shown at the top of Panels (m) and (n). The E-P flux and its divergence are calculated from wave 1 to 3. E-P flux vectors are scaled by the factor $\cos\varphi$ and multiplied by the square

255

260

root of 1000.0/p in both the vertical and horizontal directions, where p is pressure in hPa. The dotted regions indicate that the differences in (a)−(e) zonal-mean zonal wind, (f)−(j) E-P flux divergence, and (k)−(o) zonal-mean temperature are statistically significant at the 90% confidence level. Green shadings indicate that the differences in ozone volume mixing ratio between the Pos-Exmode and Neg-Exmode are statistically significant at the 90% confidence level. Only the significant (at the 90% confidence level) E-P flux vectors have been plotted in panels (f)−(j).

Additionally, negative temperature anomalies are located south of the positive anomalous zonal wind center according to the thermal wind balance. There is also a poleward and downward shift in temperature anomalies along with the anomalous zonal wind from July to November (Figs. 4k−o). Finally, the lower Antarctic stratosphere is much colder in Pos-Exmode than Neg-Exmode. In austral spring (September to November), temperature plays a crucial role in influencing the Antarctic stratospheric ozone. Lower temperature in the lower stratosphere favours increased PSC area and chemical ozone depletion in the polar regions (Figs. 4m−n). Consequently, the temperature decrease induced by the positive extratropical mode leads to negative ozone anomalies in the Antarctic lower stratosphere from September to November (Figs. 4m−o).
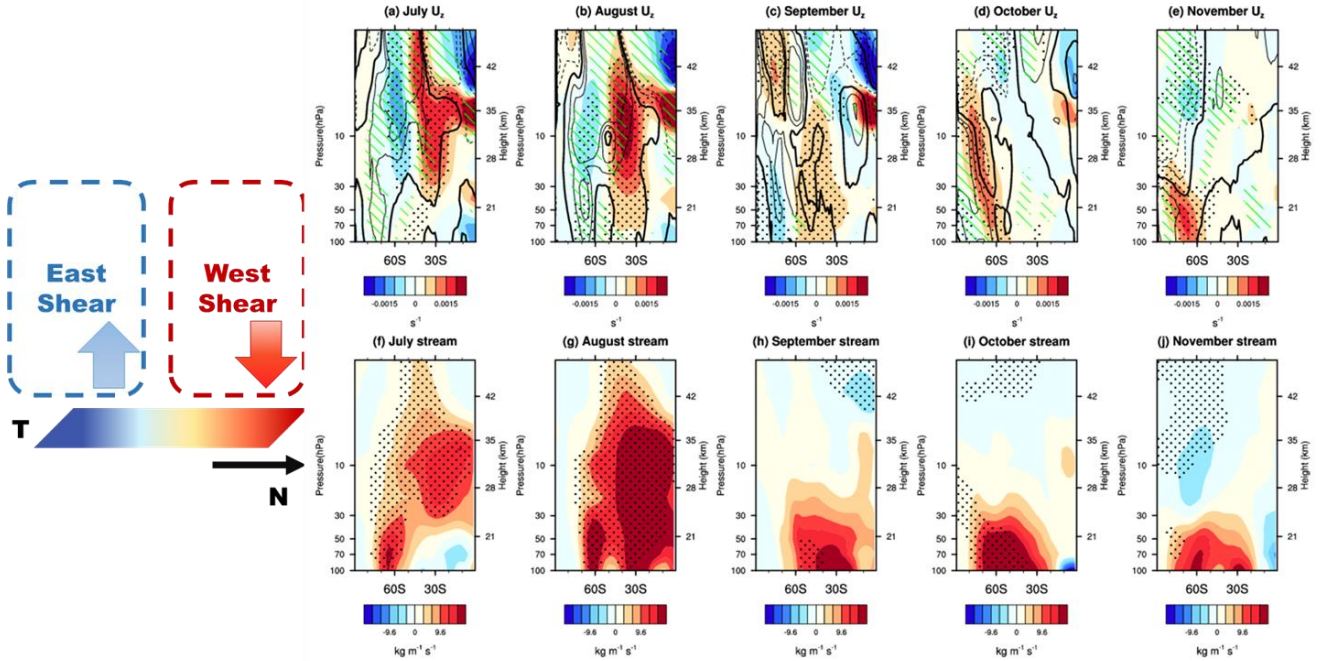
Figure 5: Composite differences in the (a)−(e) vertical gradient of zonal-mean zonal wind anomalies (shadings) and vertical component of residual mean circulation ($\overline{w}*$) anomalies (contours; dashed lines are negative, and thick lines are zero contours. The contour intervals are 0.1 mm/s), and (f)−(j) stream function anomalies from July to November between the Pos-Exmode and Neg-Exmode according to MERRA-2 reanalysis dataset. The dotted regions indicate that the differences in (a)−(e) vertical gradient of zonal-mean zonal wind and (f)−(j) stream function between the Pos-Exmode and Neg-Exmode are statistically significant at the 90% confidence level. Green shadings indicate that the differences in $\overline{w}*$ between the Pos-Exmode and Neg-Exmode are statistically significant at the 90% confidence level. The schematic diagram on the left illustrates how the secondary circulation is triggered and sustained.

There are three main processes responsible for the extratropic-polar connection during the WQBO. The first process, named as the thermal wind balance, is described as follows. The positive extratropical mode defined in Fig. 3a exhibits positive

zonal-mean zonal wind anomalies, as well as a positive vertical gradient around 30ºS (Figure 5a). Meridional temperature anomalies must exist to maintain thermal wind balance for the vertical shear of the zonal-mean zonal wind in the basic state flow. These meridional temperature anomalies are sustained by the secondary vertical motion. Specifically, a positive zonal-mean zonal wind shear anomaly (shadings in Fig. 5a), accompanied by a warm center in north of 30ºS (Fig. 4k), is maintained

290 by the downward motion (contours in Fig. 5a), while a negative zonal-mean zonal wind shear anomaly in higher latitudes accompanies a cold center and upward motion (Figs. 4k and 5a). Note that the climatological basic state meridional flow in austral spring is characterized by a negative stream function, with upward motion in the tropic and downward motion at higher latitudes (i.e., Brewer-Dobson circulation). In July and August, positive stream function anomalies appear at lower latitudes in the upper stratosphere, indicating clockwise secondary circulations induced by the extratropical mode during the WQBO

295 (Figs. 5f−g).
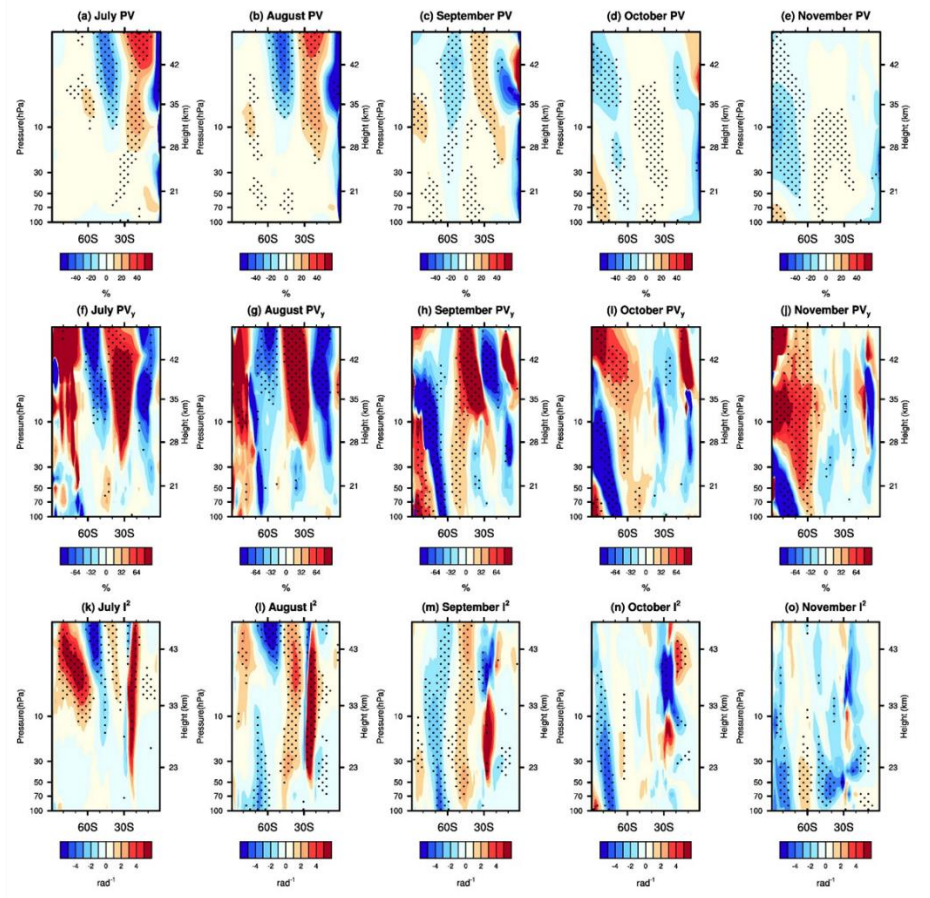
Figure 6: Composite differences in the (a)−(e) potential vorticity (PV) anomalies, (f)−(j) meridional gradient of PV anomalies, and (k)−(o) meridional component of refraction index anomalies from July to November between the Pos-Exmode and Neg-Exmode
300 **according to MERRA-2 reanalysis dataset. The dotted regions indicate that the differences in (a)−(e) PV, (f)−(j) meridional gradient of PV, and (k)−(o) meridional component of refraction index between the Pos-Exmode and Neg-Exmode are statistically significant at the 90% confidence level. The schematic diagram on the left illustrates the mechanism of the PV adjustment. The black lines indicate the climatological PV contours in the SH.**

The second process is the potential vorticity (PV) adjustment. The secondary circulation mentioned above causes vertical compression and stretching of air columns in the lower and higher latitudes, respectively. As a result, the air column will acquire anticyclone vorticity (positive PV anomalies) in lower latitudes and cyclone vorticity (negative PV anomalies) in higher latitudes (schematic diagram of Figure 6). In July, positive stream function anomalies are centered around 30ºS (Fig. 5f), resulting in positive and negative PV anomalies at 20ºS and 40ºS in the upper stratosphere, respectively (Fig. 6a). This redistribution of PV leads to negative meridional gradient of PV (PV_y) anomalies around 60ºS (Fig. 6f), which dominate the wave refractive index and results in anomalous E-P flux divergence around 50ºS in the upper stratosphere in July (Fig. 4f). In the following months, the positive center of the stream function gradually shifts toward the lower stratosphere and polar regions (Figs. 5g−j). Consequently, the induced negative PV_y anomalies and wave refractive index also exhibit a poleward and downward shift (Fig. 6). Especially from August to September, there is a notable transition in E-P flux divergence anomalies from the upper stratosphere around 60ºS to the middle and lower stratosphere (30−100 hPa; Figs. 4g−h). At the same time, both the anomalous centers of the stream function and PV_y also shift downward to the lower stratosphere (Figs. 5g−h, 6b−c, 6g−h, and 6l−m). This downward and poleward process can be interpreted as wave-mean flow interaction, as described below.
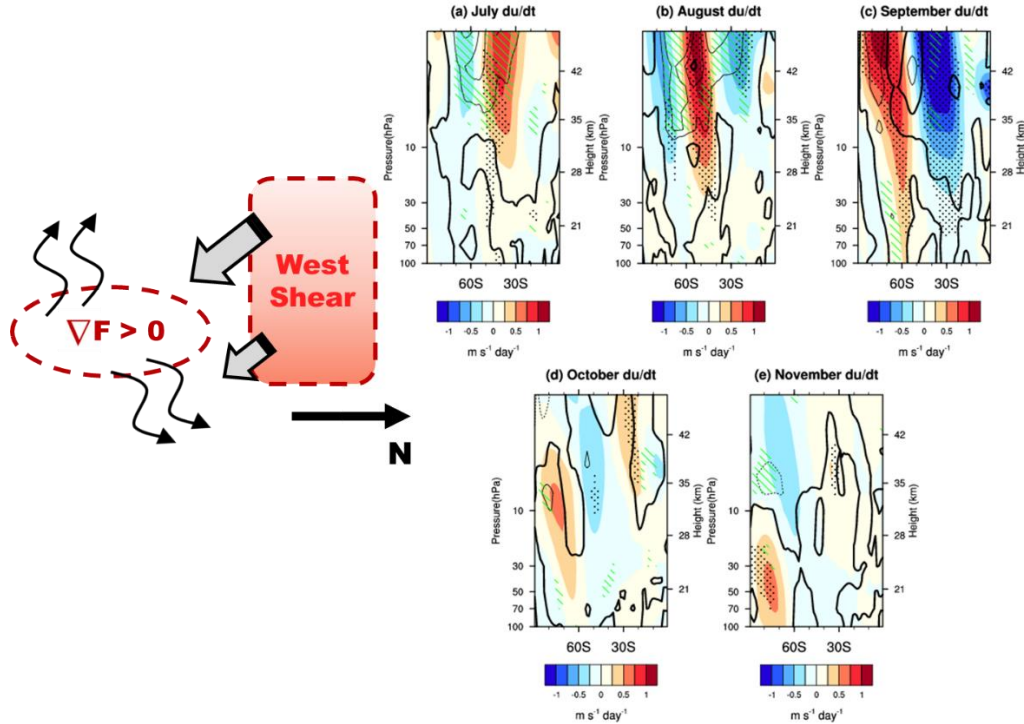
Figure 7: Composite differences in the du/dt anomalies (color shadings) and E-P flux divergence anomalies (contours; dashed lines are negative, and thick lines are zero contours. The contour intervals are 0.25 m s^{-1} day^{-1}) from July to November between the Pos-Exmode and Neg-Exmode according to MERRA-2 reanalysis dataset. The dotted regions and green shadings indicate that the differences in du/dt and the differences in E-P flux divergence between the Pos-Exmode and Neg-Exmode are statistically significant at the 90% confidence level. The schematic diagram illustrates how these anomalies propagate towards the Antarctic lower stratosphere from July to November.

The wave-mean flow interaction sustains the anomalies mentioned above propagating towards the Antarctic lower
325 stratosphere from July to November (schematic diagram of Figure 7). Specifically, in July, the anomalous E-P flux divergence
centered around 50ºS in the upper stratosphere (Fig. 7a) induces a poleward and downward shift of the positive anomalous
zonal-mean zonal wind (positive anomalies of du/dt), along with other anomalous centers. In the following months, the
anomalous E-P flux divergence, as well as the positive du/dt anomalies, continue to move towards the lower stratosphere in
the polar region. By November, the center of positive zonal-mean zonal wind anomaly is located in the polar region in the
330 mid-stratosphere (Fig. 4e), indicating a stronger and colder polar vortex.
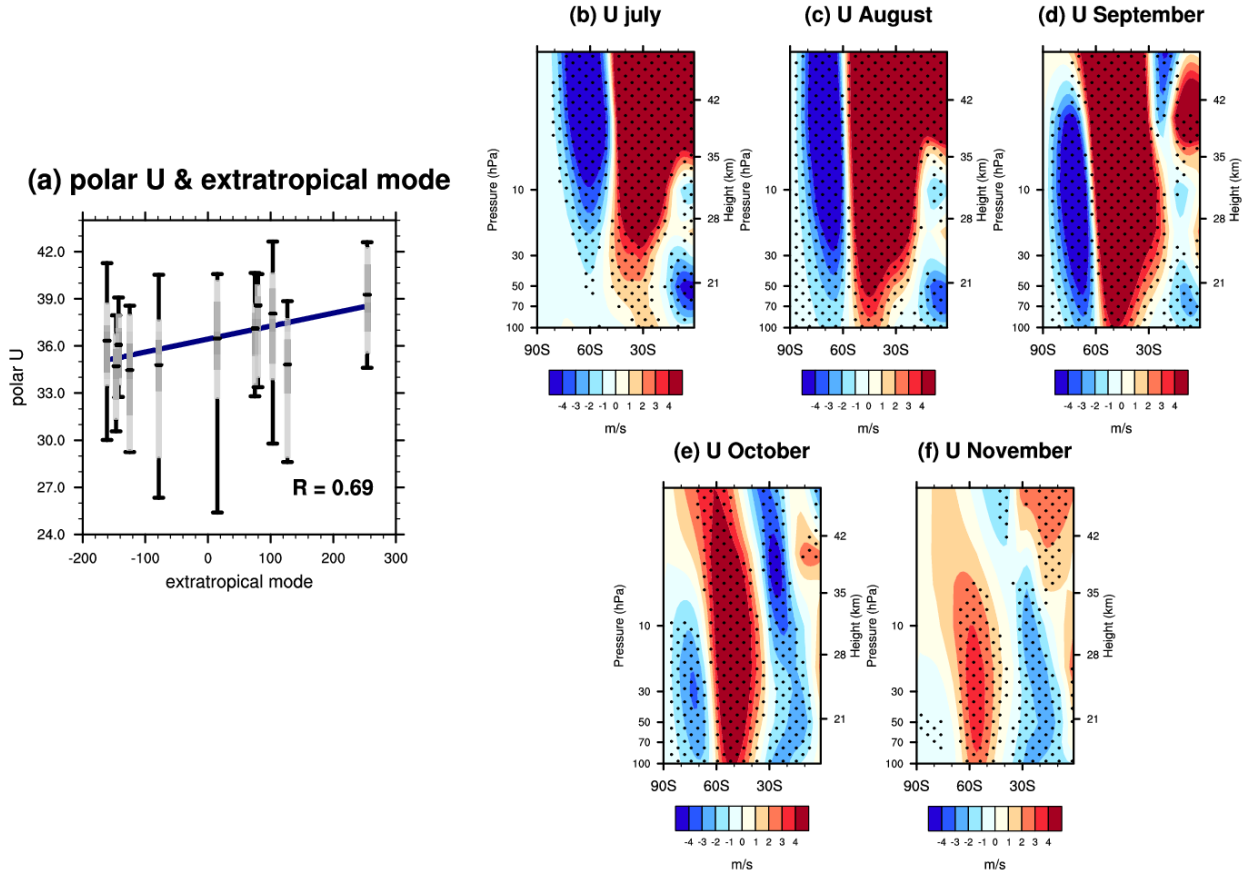
Figure 8: (a) The zonal-mean zonal wind at 60ºS and 100 hPa in November is plotted against the extratropical mode's PC in July
during WQBO years, derived from the 20 ensembles of CESM simulation. The boxplot describes a summary of these ensembles.
335 The light grey box spans from the lower decile to the upper decile, and the dark grey spans the lower quartile to upper quartile.
The lines inside the dark grey box marks the median zonal wind. The lower and upper whiskers indicate the minimum and maximum
zonal wind among the 20 ensembles. Additionally, the blue line represents the linear fit between the extratropical mode and the
median zonal wind, with their correlation coefficient displayed in the bottom right-hand corner. (b)−(f) Composite differences in
zonal-mean zonal wind from July to November between the Pos-Exmode and Neg-Exmode according to CESM simulations. The
340 dotted regions indicate that the differences between the Pos-Exmode and Neg-Exmode are statistically significant at the 95%
confidence level.

Based on the abovementioned analyses, we proposed a new predictor for the Antarctic stratospheric vortex in spring. During the WQBO, the correlation between the extratropical mode and polar vortex can reach 0.75 with a five-month time lag. To further verify these results, additional model experiments are conducted by the CESM2. First, the relation between the extratropical mode in July and the Antarctic stratospheric polar vortex in November has been validated. Figure 8a shows the zonal-mean zonal wind at 60ºS in November as a function of the extratropical mode in July, derived from the 20 ensembles during the WQBO. Similar to the reanalysis dataset (Fig. 3c), the strength of the Antarctic polar vortex increases with a larger extratropical mode, with a correlation reaching 0.69. We further display the composite results of the zonal-mean zonal wind (Figs. 8b−f). For each ensemble, the years in Pos-Exmode and Neg-Exmode are selected, and the difference in zonal-mean zonal wind between Pos-Exmode and Neg-Exmode is calculated across all ensembles. Initially, positive zonal-mean zonal wind anomalies appear around 30ºS in the upper stratosphere in July (Fig. 8b). These anomalies gradually shift to the lower stratosphere and polar regions due to wave-mean flow interactions (Figs. 8c−e), ultimately resulting in a stronger polar vortex in the Antarctic lower stratosphere by November (Fig. 8f). The continuous evolution of these positive anomalous zonal-mean zonal wind from the extratropical upper stratosphere to the Antarctic lower stratosphere indicates a robust relationship between the extratropical mode and the Antarctic polar vortex during the WQBO.
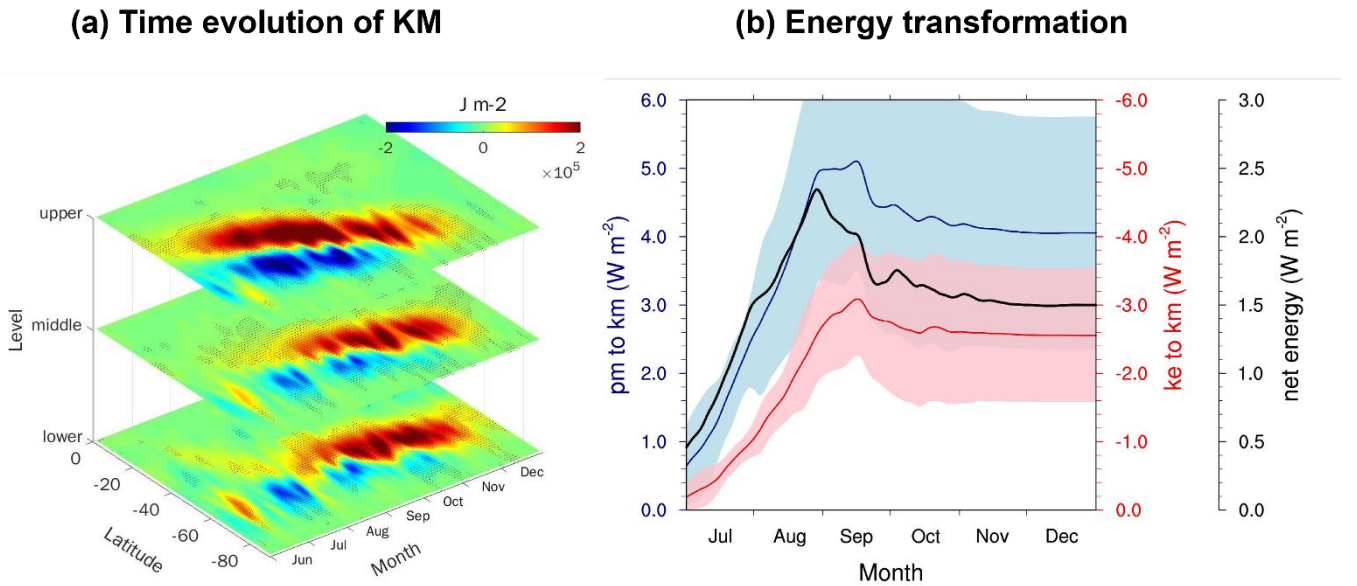
Figure 9: (a) Composite differences in mean kinetic energy (KM) from July to November between the Pos-Exmode and Neg-Exmod according to MERRA-2 reanalysis dataset. The KM at "upper", "middle", and "lower" levels are integrated 1−20 hPa, 30−50 hPa, and 70−100 hPa, respectively. The dotted regions indicate that the differences between the Pos-Exmode and Neg-Exmode are statistically significant at the 90% confidence level. (b) Composite differences in time-integrated energy transformations averaged over 1−100 hPa and 40ºS−70ºS between the Pos-Exmode and Neg-Exmode. The blue and red shadings indicate significant intervals. If these shadings do not cross the X-axis, the difference is significant at the 90% confidence level. The blue line, corresponding to the left Y-axis, represents the energy transformed from the mean potential energy (PM) to KM. The red line, corresponding to the first right Y-axis, represents the energy transformed from the eddy kinetic energy (KE) to KM. The black line, corresponding to the second right Y-axis, represents the net energy transformed to KM.
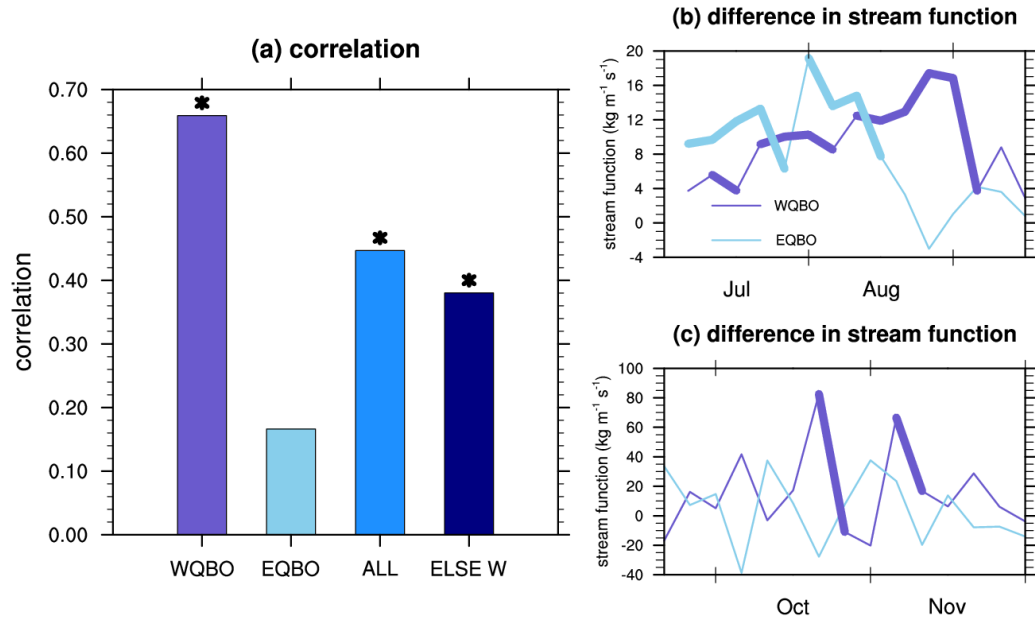
**Figure 10: (a) The correlations between zonal-mean zonal wind in extratropical and polar regions during WQBO years (WQBO),
EQBO years (EQBO), all years (ALL), and years except WQBO (ELSE W) derived from MERRA-2 reanalysis dataset from 1980
to 2022. The asterisks indicate that the correlations are statistically significant at the 95% confidence level. (b) Composite differences
in stream function averaged over 0−60ºS and 1−30 hPa between the strong and weak polar vortex during the WQBO (purple lines)
and EQBO (blue lines) from July to September. The thick lines indicate that the differences between the strong and weak polar
vortex are statistically significant at the 90% confidence level. (c) Same as panel (b), but the stream function averaged over 30ºS
−60ºS and 50−100 hPa from September to November.**

A question arises as to why the abovementioned wave-mean flow interactions could persist for almost five months. We

attempt to explain it from the perspective of the Lorenz energy cycle. Lorenz (1967) proposed that the solar energy is converted

into the available potential energy, which then drives kinetic energy to maintain atmospheric circulation against both thermal

and mechanical dissipations. As a result, the Lorenz energy cycle reflects changes in atmospheric circulation. Figure 9a

displays the evolution of KM from June to December, which is proportional to the square of the zonal-mean zonal wind ($\overline{u}^{2}$)

and, therefore, effectively captures the transition of atmospheric circulation depicted in Figs. 4a−e. Positive KM anomalies

originated in the mid-latitudes in upper stratosphere at the end of June and then propagate poleward and downward until

November. This evolution of KM suggests a continuous anomalous energy transfer from the mid latitudes in upper stratosphere

to the polar regions, sustaining the positive zonal-mean zonal wind anomalies observed in Pos-Exmode. Next, we explain why

the positive anomalies in KM can persist for almost five months (Fig. 9b). Note that the KM is primarily maintained by

conversion from KE (Eq. 11) and PM (Eq. 12). There is a continuous anomalous conversion from PM to KM since July (blue

line, Y-axis in the left), which is corresponding to the secondary circulation in Figs. 5f−j. In July, the positive stream function

anomalies around 30ºS at 20 hPa (Fig. 5f) indicates a clockwise secondary circulation. This circulation lifts the anomalous

warmer air at 50°S to higher altitudes (Fig. 4k), lowing the center of mass. Consequently, more potential energy is converted

390 into kinetic energy in Pos-Exmode over the mid-latitudes (Fig. 9b). The following months are similar to this process. In addition, KM is also maintained by the conversion from KE. In Pos-Exmode, weak wave activities (Figs. 4f–j) result in less KE being converted into KM compared to Neg-Exmode (red line, first Y-axis in the right). The positive conversion rate from PM to KM is greater than that from KE to KM. As a result, more energy is stored in KM during Pos-Exmode compared to Neg-Exmode.

395   Note that this relationship only exists under WQBO conditions. The correlations between the extratropical mode in July and Antarctic polar vortex in November can reach 0.65 during WQBO, but it is as low as 0.15 in EQBO (Figure 10a). This is due to the intrinsic difference in B-D circulation between WQBO and EQBO, driven by the variation in the vertical gradient of the zonal-mean zonal wind in the tropical upper stratosphere (Figure 11). Compared with EQBO, there are anomalous descending motions around 15°S at 10 hPa in WQBO, which facilitate the formation and maintenance of the secondary

400 circulation (Figs. 5f–j). Therefore, during the WQBO, the secondary circulation, as well as other anomalous centers, propagate downward and poleward, especially from September to November. In contrast, during EQBO, the anomalous ascending motions in the tropic offset the secondary circulations induced by the extratropic mode, and thus the secondary circulation weakens and gradually dissipate. Figs. 10b and c illustrate the composite difference in the spatial integral stream function. Note that at the beginning of July, the anomalous secondary circulation is stronger in EQBO than in WQBO. However, the

405 extratropic-polar connection gradually disrupts from September in EQBO.
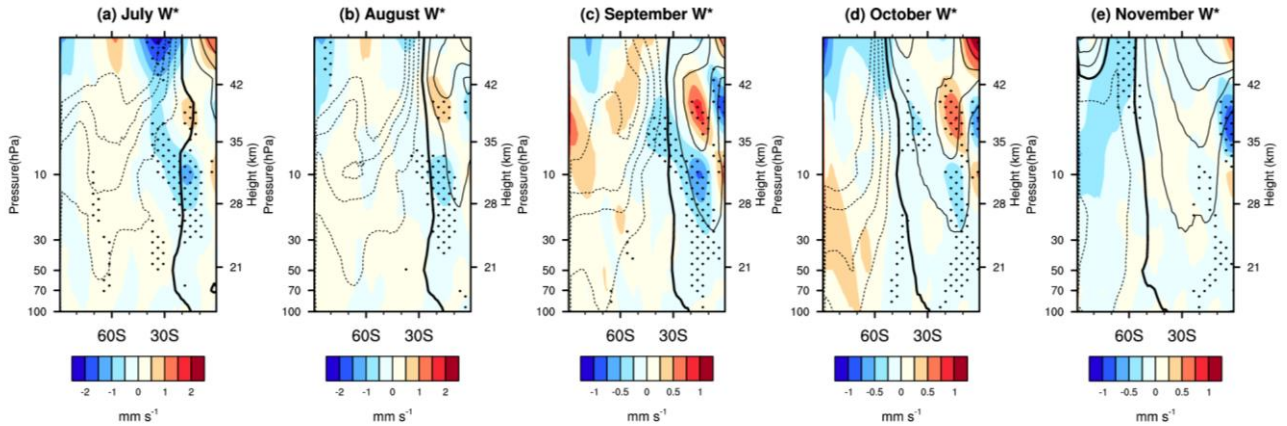
Figure 11: Composite differences (color shadings) in $\overline{w}*$ between WQBO and EQBO from July and November according to the MERRA-2 reanalysis dataset. The dotted regions indicate that the differences in $\overline{w}*$ between the WQBO and EQBO are statistically significant at the 90% confidence level. The contours indicate the climatological $\overline{w}*$ from 1980 to 2022. The dashed lines are
410 **negative. Thick lines are zero contours, and the contour intervals are 0.5 mm/s.**

4 Conclusion and discussion

  The dynamical coupling between high and low latitudes has been widely discussed. However, no studies have pointed out a robust connection between the QBO and the Antarctic stratospheric polar vortex, as well as the Antarctic ozone. In this

study, we used the MERRA-2 reanalysis data and CESM model simulations to investigate the relationship between the QBO
and the Antarctic stratospheric polar vortex.

During the WQBO, positive zonal-mean zonal wind anomalies at 20°S−40°S in the upper stratosphere in July, named as the positive extratropical mode (Figs. 2 and 3a), lead to a stronger polar vortex in November, with a correlation reaching 0.75 (Fig. 3c). The positive extratropical mode can trigger a secondary circulation (Figs. 5f−j). The anomalous downward motions in lower latitudes and upward motions in higher latitudes cause anomalous meridional gradient of PV (Figs. 6a−j), which further alters the environmental condition for wave propagation in the stratosphere (Figs. 6k−o), pushing the positive zonal-mean zonal wind anomalies towards the pole (Fig. 7). It takes nearly five months for the positive zonal-mean zonal wind anomalies to propagate from 30°S to 60°S. Additionally, the anomalous Antarctic stratospheric polar vortex induced by the extratropical mode, along with the anomalous temperature in Antarctic stratospheric regions, can influence the Antarctic ozone hole in austral spring (Figs. 4m−o). This results in a high correlation between the extratropical mode in July and the Antarctic ozone concentration in November (Fig. 3c). Therefore, based on the relation between the extratropical mode and the strength of Antarctic polar vortex, the extratropical mode can be regarded as a predictor of the Antarctic stratospheric polar vortex and ozone in austral spring during the WQBO. However, the reasons why the extratropical mode varies and its potential relationship with the QBO phase warrant further investigation.

During EQBO, the correlation of the extratropical mode and the strength of polar vortex is only 0.15 (Fig. 10a). Due to stronger upward motions in the tropics, which oppose the secondary circulation caused by the extratropical mode, the EQBO can only sustain the positive zonal-mean zonal wind anomalies until September. Therefore, further analysis is needed to find a realistic connection between the EQBO and the polar vortex.

As mentioned in the literature review, QBO through the middle and lower stratospheric pathway impacts the stratospheric polar vortex (Naoe and Shibata, 2010; Yamashita et al., 2011; 2018). In this study, we propose an upper stratospheric pathway for the QBO's impact on the Antarctic stratospheric polar vortex, which can persist for nearly five months. This suggests that the Antarctic stratospheric polar vortex and ozone concentration in austral spring can be predicted up to five months in advance. Additionally, it is generally recognized that the EQBO has a greater influence on the stratospheric polar vortex than the WQBO. However, through the upper stratospheric pathway, the WQBO during austral winter, combined with the extratropical zonal-mean zonal wind in the upper stratosphere, are highly correlated with the Antarctic stratospheric polar vortex and ozone in spring.

Data availability: MERRA-2 data are available at https://disc.gsfc.nasa.gov/datasets?project=MERRA-2. The PSC area data can be obtained from https://ozonewatch.gsfc.nasa.gov/. The code used in this article is accessible from the corresponding author.

Author contributions: All authors designed the study. ZW analysed and prepared the data for the paper. JZ, ZW, DL, and SZ contributed to data interpretation and writing of the paper.

Competing interests: The authors declare that they have no conflict of interest.

Acknowledgements: We thank Dr. Yamashita, the editor, and the two anonymous reviewers for their helpful comments. This research is supported by the National Natural Science Foundation of China (U2442211, 42075062, 42130601). We thank the scientific teams at National Aeronautics and Space Administration (NASA) for providing the MERRA-2 reanalysis data. We thank the NCAR For the CESM2 model. We gratefully acknowledge Dr. Nili Harnik for providing the code of the quasigeostrophic model to calculate the index of refraction. We also appreciate the computing support provided by the Supercomputing Center of Lanzhou University.

References

Andrews, D. G. and McIntyre, M. E.: Planetary waves in horizontal and vertical shear: The generalized Eliassen–Palm relation and the mean zonal acceleration, J. Atmos. Sci., 33, 2031–2048, https://doi.org/10.1175/1520-0469(1976)033<2031:PWIHAV>2.0.CO;2 1976.

Andrews, M. B., Knight, J. R., Scaife, A. A., Lu, Y., Wu, T., Gray, L. J. and Schenzinger, V.: Observed and simulated teleconnections between the stratospheric quasi-biennial oscillation and Northern Hemisphere winter atmospheric circulation, J. Geophys. Res. Atmos., 124, 1219–1232, https://doi.org/10.1029/2018JD029368. 2019.

Anstey, J. A., Shepherd, T. G. and Scinocca, J. F.: Influence of the quasi-biennial oscillation on the extratropical winter stratosphere in an atmospheric general circulation model and in reanalysis data, J. Atmos. Sci., 67, 1402–1419, https://doi.org/10.1175/2009JAS3292.1, 2010.

Anstey, J. A. and Shepherd, T. G.: High-latitude influence of the quasi-biennial oscillation, Q. J. R. Meteorol. Soc., 140, 1−21, https://doi.org/10.1002/qj.2132, 2014.

Anstey, J.A. et al.: Teleconnections of the Quasi-Biennial Oscillation in a multi-model ensemble of QBO-resolving models. Q. J. R. Meteorol. Soc, 148, 1568–1592, https://doi.org/10.1002/qj.4048, 2022.

Baldwin, M. P. and Dunkerton, T. J.: Quasi-biennial modulation of the southern hemisphere stratospheric polar vortex, Geophys. Res. Lett., 25, 3343–3346, https://doi.org/10.1029/98GL02445, 1998.

Baldwin, M. P., Gray, L. J., Dunkerton, T. J., Hamilton, K, Haynes, P. H., Randel, W. J., Holton, J. R., Alexander, M. J., Hirota, I., Horinouchi, T., Jones, D. B. A., Kinnersley, J. S., Marquardt, C., Sato, K. and Takahashi, M.: The quasi-biennial oscillation, Rev. Geophys., 39, 179–229, https://doi.org/10.1029/1999RG000073, 2001.

Davis, N. A., Callaghan, P., Simpson, I. R. and Tilmes, S.: Specified dynamics scheme impacts on wave-mean flow dynamics, convection, and tracer transport in CESM2 (WACCM6), Atmos. Chem. Phys., 22, 197–214, https://doi.org/10.5194/acp-22-197-2022, 2022.

475   Garcia, R. R. and Solomon, S.: A possible relationship between interannual variability in Antarctic ozone and the quasi-biennial oscillation, Geophys. Res. Lett., 14, 848–851, https://doi.org/10.1029/GL014i008p00848, 1987.

Garfinkel, C. I. and Hartmann, D. L.: Different ENSO teleconnections and their effects on the stratospheric polar vortex, J. Geophys. Res., 113, D18114, https://doi.org/10.1029/2008JD009920, 2008.

Garfinkel, C. I. and Hartmann, D. L.: The Influence of the Quasi-Biennial Oscillation on the troposphere in winter in a hierarchy of models. Part I: Simplified dry GCMs, J. Atmos. Sci., 68, 1273−1289, https://doi.org/10.1175/2011JAS3665.1, 480   2011.

Garfinkel, C. I., Shaw, T. A., Hartmann, D. L. and Waugh, D. W.: Does the Holton–Tan mechanism explain how the Quasi-Biennial Oscillation modulates the Arctic polar vortex? J. Atmos. Sci., 69, 1713−1733, https://doi.org/10.1175/JAS-D-11-0209.1, 2012.

Global Modeling and Assimilation Office (GMAO) (2015), inst3_3d_asm_Cp: MERRA-2 3D IAU State, Meteorology 485   Instantaneous 3-hourly (p-coord, 1.25x1.25L42), version 5.12.4, Greenbelt, MD, USA: Goddard Space Flight Center Distributed Active Archive Center (GSFC DAAC), Accessed Enter User Data Access Date at https://doi.org/10.5067/QBZ6MG944HW0.

Gray, W. M., Sheaffer, J. D. and Knaff, J. A.: Hypothesized mechanism for stratospheric QBO influence on ENSO variability, Geophys. Res. Lett., 19, 107–110, https://doi.org/10.1029/91GL02950, 1992.

490   Gray, L. J., Anstey, J. A., Kawatani, Y., Lu, H., Osprey, S. and Schenzinger, V.: Surface impacts of the Quasi Biennial Oscillation, Atmos. Chem. Phys., 18, 8227−8247, https://doi.org/10.5194/acp-18-8227-2018, 2018.

Gettelman, A., Mills, M. J., Kinnison, D. E., Garcia, R. R., Smith, A. K., Marsh, D. R., Tilmes, S., Vitt, F., Bardeen, C. G., McInerny, J., Liu, H. -L., Solomon, S. C., Polvani, L. M., Emmons, L. K., Lamarque, J. -F., Richter, J. H., Glanville, A. S., Bacmeister, J. T., Phillips, A. S., Neale, R. B., Simpson, I. R., DuVivier, A. K., Hodzic, A. and Randel, W. J.: The whole 495   atmosphere community climate model version 6 (WACCM6), J. Geophys. Res. Atmos., 124, 12380–12403, https://doi.org/10.1029/2019JD030943, 2019.

Garfinkel, C. I. and Hartmann, D. L.: Effects of the El Niño–Southern Oscillation and the quasi-biennial oscillation on polar temperatures in the stratosphere, J. Geophys. Res., 112, D19112, https://doi.org/10.1029/2007JD008481, 2007.

Holton, J. R. and Hakim, G. J.: An Introduction to Dynamic Meteorology, Academic Press, 248 pp, 1973.

500   Holton, J. R. and Tan, H. C.: The influence of the equatorial quasi-biennial oscillation on the global circulation at 50 mb, J. Atmos. Sci., 37, 2200–2208, https://doi.org/10.1175/1520-0469(1980)037<2200:TIOTEQ>2.0.CO;2, 1980.

Hu, Q., Tawaye, Y. and Feng, S.: Variations of the Northern Hemisphere Atmospheric Energetics: 1948–2000, J. Climate, 17, 1975–1986, https://doi.org/10.1175/1520-0442(2004)017<1975:VOTNHA>2.0.CO;2, 2004.

Hitchman, M. H. and Huesmann, A. S.: Seasonal influence of the quasi-biennial oscillation on stratospheric jets and Rossby wave breaking, J. Atmos. Sci., 66, 935–946, https://doi.org/10.1175/2008JAS2631.1, 2004.

Harnik, N. and Lindzen, R. S.: The effect of reflecting surfaces on the vertical structure and variability of stratospheric planetary waves, J. Atmos. Sci., 58, 2872–2894, https://doi.org/10.1175/1520-0469(2001)058<2872:TEORSO>2.0.CO;2, 2001.

Iwasaka, N. and Wallace, J. M.: Large scale air sea interaction in the Northern Hemisphere from a view point of variations of surface heat flux by SVD analysis, J. Meteorol. Soc. Jpn., 73, 781–794, https://doi.org/10.2151/jmsj1965.73.4_781, 2001.

Lorenz, E. N.: The Nature and Theory of the General Circulation of the Atmosphere. World Meteorological Organization, 161 pp, 1967.

Lindzen, R. S. and Holton, J. R.: A theory of the quasi-biennial oscillation, J. Atmos. Sci., 25, 1095–1107, https://doi.org/10.1175/1520-0469(1968)025<1095:ATOTQB>2.0.CO;2, 1968.

Lait, L. R., Schoeberl, M. R. and Newman, P. A.: Quasi-biennial modulation of the Antarctic ozone depletion, J. Geophys. Res., 94, 11559–11571, https://doi.org/10.1029/JD094iD09p11559, 1989.

Lu, H., Bracegirdle, T. J., Phillips, T., Bushell, A. and Gray, L.: Mechanisms for the Holton-Tan relationship and its decadal variation, J. Geophys. Res. Atmos., 119, 2811–2830, https://doi.org/10.1002/2013JD021352, 2014.

Lecouffe, A., Godin-Beekmann, S., Pazmiño, A. and Hauchecorne, A.: Evolution of the intensity and duration of the Southern Hemisphere stratospheric polar vortex edge for the period 1979–2020, Atmos. Chem. Phys., 22, 4187–4200, https://doi.org/10.5194/acp-22-4187-2022, 2022.

Lu, Q., Rao, J., Shi, C. H., Ren, R. C., Liu, Y. M. and L, S. M.: Stratosphere-troposphere coupling during stratospheric extremes in the 2022/23 winter, Weather Clim. Extrem., 42, 100627, https://doi.org/10.1016/j.wace.2023.100627, 2023.

Matsuno, T.: Vertical Propagation of Stationary Planetary Waves in the Winter Northern Hemisphere, J. Atmos. Sci., 27, 871–883, https://doi.org/10.1175/1520-0469(1970)027<0871:VPOSPW>2.0.CO;2, 1970.

Naito, Y.: Planetary wave diagnostics on the QBO effects on the deceleration of the polar-night jet in the southern hemisphere, J. Meteor. Soc. Japan, 80, 985–995, https://doi.org/10.2151/JMSJ.80.985, 2002.

Naoe, H. and Shibata, K.: Equatorial quasi-biennial oscillation influence on northern winter extratropical circulation, J. Geophys. Res., 115, D19102, https://doi.org/10.1029/2009JD012952, 2010.

Randel, W. J., Wu, F., Swinbank, R., Nash, J. and O'Neill, A.: Global QBO circulation derived from UKMO stratospheric analyses, J. Atmos. Sci., 56, 457–474, https://doi.org/10.1175/1520-0469(1999)056<0457:GQCDFU>2.0.CO;2, 1999.

Ruti, P. M., Lucarini, V., Dell'Aquila, A., Calmanti, S. and Speranza, A.: Does the subtropical jet catalyze the midlatitude atmospheric regimes? Geophys. Res. Lett., 33, L06814, https://doi.org/10.1029/2005GL024620, 2006.

Rao, J. and Ren, R.-C.: Varying stratospheric responses to tropical Atlantic SST forcing from early to late winter, Climate Dyn., 51, 2079–2096, https://doi.org/10.1007/s00382-017-3998-x, 2018

Rao, J., Yu, Y., Guo, D., Shi, C., Chen, D. and Hu, D.: Evaluating the Brewer–Dobson circulation and its responses to ENSO, QBO, and the solar cycle in different reanalyses, Earth planet. phys., 3, 166–181, https://doi.org/10.26464/epp2019012, 2019.

Rao, J., Garfinkel, C. I. and White, I. P.: Projected strengthening of the extratropical surface impacts of the stratospheric quasi-biennial oscillation, Geophys. Res. Lett., 47, e2020GL089149, https://doi.org/10.1029/2020GL089149, 2020a.

540 Rao, J., Garfinkel, C. I. and White, I. P.: Impact of the Quasi-Biennial Oscillation on the Northern Winter Stratospheric Polar Vortex in CMIP5/6 Models, J. Climate, 33, 4787–4813, https://doi.org/10.1175/JCLI-D-19-0663.1, 2020b.

Rao, J., Garfinkel, C. I. and White, I. P.: How Does the Quasi-Biennial Oscillation Affect the Boreal Winter Tropospheric Circulation in CMIP5/6 Models?. J. Climate, 33, 8975–8996, https://doi.org/10.1175/JCLI-D-20-0024.1, 2020c.

Rao, J., Garfinkel, C. I., Ren, R., Wu, T. and Lu, Y.: Southern Hemisphere Response to the Quasi-Biennial Oscillation in the

545 CMIP5/6 Models. J. Climate, 36, 2603–2623, https://doi.org/10.1175/JCLI-D-22-0675.1,2023a.

Rao, J., Garfinkel, C. I., Ren, R., Wu, T., Lu, Y. and Chu, M.: Projected Strengthening Impact of the Quasi-Biennial Oscillation on the Southern Hemisphere by CMIP5/6 Models. J. Climate, 36, 5461–5476, https://doi.org/10.1175/JCLI-D-22-0801.1, 2023b.

Tian, W. S., Chipperfield, M. P., Gray, L. J. and Zawodny, J. M.: Quasi-biennial oscillation and tracer distributions in a coupled

550 chemistry-climate model, J. Geophys. Res., 111, D20301, https://doi.org/10.1029/2005JD006871, 2006.

Tian, W. S., Huang, J. L., Zhang, J. K., Xie, F., Wang, W. K. and Peng, Y. F.: Role of Stratospheric Processes in Climate Change: Advances and Challenges, Adv. Atmos. Sci., 40, 1379–1400, https://doi.org/10.1007/s00376-023-2341-1, 2023.

Wang W. K., Hong, J., Shangguan, M., Wang, H. Y., Jiang W. and Zhao S. Y.: Zonally asymmetric influences of the quasi-biennial oscillation on stratospheric ozone, Atmos. Chem. Phys., 22, 13695–13711, https://doi.org/10.5194/acp-22-13695-

555 2022, 2022.

Yamashita, Y., Akiyoshi, H. and Takahashi, M.: Dynamical response in the Northern Hemisphere midlatitude and high-latitude winter to the QBO simulated by CCSR/NIES CCM, J. Geophys. Res., 116, D06118, https://doi.org/10.1029/2010JD015016, 2011.

Yamashita, Y., Akiyoshi, H., Shepherd, T. and Takahashi, M.: The Combined Influences of Westerly Phase of the Quasi-

560 Biennial Oscillation and 11-year Solar Maximum Conditions on the Northern Hemisphere Extratropical Winter Circulation, J. Meteorol. Soc. Jpn., 93, 6, 629−644, https://doi.org/10.2151/jmsj.2015-054, 2015.

Yamashita, Y., Naoe, H., Inoue, M. and Takahashi, M.: Response of the Southern Hemisphere Atmosphere to the Stratospheric Equatorial Quasi-Biennial Oscillation (QBO) from Winter to Early Summer, J. Meteorol. Soc. Jpn., 96, 6, 587−600, https://doi.org/10.2151/jmsj.2018-057, 2018.

565 Zhang, J. K., Xie, F., Ma, Z. C., Zhang, C. Y., Xu, M., Wang, T. and Zhang, R. H.: Seasonal evolution of the quasi-biennial oscillation impact on the Northern Hemisphere polar vortex in winter, J. Geophys. Res. -Atmos., 124, 12568–12586, https://doi.org/10.1029/2019JD030966, 2019.

Zhang, R. H., Tian, W. S. and Wang, T.: Role of the quasi-biennial oscillation in the downward extension of stratospheric northern annular mode anomalies, Climate Dyn., 55, 595−612, https://doi.org/10.1007/s00382-020-05285-4, 2020.

570 Zhang, R. H., Zhou W., Tian, W. S., Zhang, Y., Zhang, J. X. and Luo, J. L.: A stratospheric precursor of East Asian summer droughts and floods, Nat. Commun., 15, 247, https://doi.org/10.1038/s41467-023-44445-y, 2024.